Journal of Alloys and Compounds 511 (2012) 115–122

Contents lists available at SciVerse ScienceDirect

Journal of Alloys and Compounds

journal homepage: www.elsevier.com/locate/jallcom

Influence of solution pH in electrodeposited iron diselenide thin films

S. Thanikaikarasan[a,*], T. Mahalingam[b]

[a] Centre for Scientific and Applied Research, School of Basic Engineering and Sciences, PSN College of Engineering and Technology, Tirunelveli 627 152, Tamil Nadu, India
[b] Department of Physics, Alagappa University, Karaikudi 630 003, Tamil Nadu, India

ARTICLE INFO

Article history:
Received 11 July 2011
Received in revised form 31 August 2011
Accepted 3 September 2011
Available online 10 September 2011

Keywords:
Thin films
X-ray diffraction
rms microstrain
Microstructure
Atomic force microscopy
Optical properties

ABSTRACT

Thin films of iron diselenide ($FeSe_2$) have been prepared on indium doped tin oxide coated conducting glass (ITO) substrates from an aqueous electrolytic bath containing $FeSO_4$ and SeO_2. Growth mechanism has been analyzed using cyclic voltammetry. The potential region in which the formation of $FeSe_2$ occurs is found to be −450 mV versus SCE. X-ray diffraction analysis showed that the deposited films are found to exhibit orthorhombic structure with preferential orientation along (1 2 0) plane. X-ray line profile analysis has been carried out to determine the microstructural parameters such as crystallite size, rms microstrain, dislocation density and stacking fault probability. Surface morphology and film composition have been analyzed using scanning electron microscopy, atomic force microscopy and energy dispersive analysis by X-rays, respectively. Optical parameters such as band gap, refractive index, extinction coefficient, real and imaginary dielectric constants, dielectric susceptibility and optical conductivity have been determined from optical absorption measurements. The observed results are discussed in detail.

1. Introduction

Thin films of semiconducting chalcogenides have attracted many researchers around the world due to their wide range of applications in photovoltaic, opto-electronic devices, photodetectors and solar energy converters [1–4]. Recently, much attention has been given to iron chalcogenides, because of their various applications in magneto-electronics, spintronics and solar cells [5–7]. Iron diselenide ($FeSe_2$) is found to be an p-type semiconducting material with a band gap value 1.03 eV which make them quite interesting for tandem solar cells [7–9,12]. Thin films of $FeSe_2$ are usually crystallized in orthorhombic marcasite type structure (JCPDS-ICDD 2003, PDF No. 21-0432) with lattice constants (a = 4.801 Å; b = 5.776 Å; c = 3.585 Å) and in the cubic structure (JCPDS-ICDD 2003, PDF No. 48-1881) with lattice constant (a = 5.776 Å). Harada has investigated the transport properties of iron dichalcogenides such as FeS_2, $FeSe_2$ and $FeTe_2$ [9]. Ouertani et al. [10,11] have obtained $FeSe_2$ thin films from sprayed amorphous iron oxide films using selenization process and investigated their structural, morphological, compositional, electrical and optical properties. Preparation of $FeSe_2$ thin films using soft selenization of iron films and their properties has been investigated using X-ray diffraction, scanning electron microscopy and X-ray photoelectron spectroscopic techniques by Hamdadou et al. [12]. An analysis of published data indicates that large number of literature is available regarding FeS_2 thin films, but very few reports are available on $FeSe_2$ and $FeTe_2$ thin films. When compared to the deposition techniques used for $FeSe_2$ film preparation mentioned above, electrodeposition appears to be attractive due to its low cost of synthesis, low temperature growth, convenience for producing large area devices and its possibility to control the film thickness and morphology by readily adjusting the electrical parameters as well as composition of the electrolytic solution [1,3,13]. Very few research reports are available regarding growth and characterization of $FeSe_2$ thin films by electrodeposition technique [7,8]. To the best of our knowledge, there is no such report is available for studying solution pH effect in electrodeposited $FeSe_2$ thin films. Hence, we have planned to carry out a systematic investigation of solution pH effect on electrochemical deposition and characterization of $FeSe_2$ thin films.

In the present work, thin films of $FeSe_2$ have been deposited on indium doped tin oxide coated conducting glass (ITO) substrates at various solution pH values. The deposition mechanism has been analyzed using cyclic voltammetry. X-ray diffraction analysis has been carried out to determine the structural properties of the deposited films. Microstructural parameters such as crystallite size, rms microstrain and dislocation density have been estimated from X-ray diffraction data using X-ray line profile analysis technique. Surface morphology, film composition and optical properties have been analyzed using scanning electron microscopy, atomic force microscopy, energy dispersive analysis by X-ray spectroscopy and optical absorption techniques, respectively. The effect of solution pH on structural, microstructural, morphological, compositional

* Corresponding author.
E-mail addresses: S_thanikai@rediffmail.com (S. Thanikaikarasan), maha51@rediffmail.com (T. Mahalingam).

0925-8388/$ – see front matter © 2011 Elsevier B.V. All rights reserved.
doi:10.1016/j.jallcom.2011.09.003

and optical properties of the films are studied. The observed results are discussed in detail.

2. Experimental details

Thin films of $FeSe_2$ were deposited on ITO substrates from an aqueous electrolytic bath containing 0.02 M $FeSO_4$ and 0.01 M SeO_2. The chemicals used in the present work were of Analar Grade Reagents (Procured from SD Fine Chemicals, Mumbai, India). The first working solution of $FeSO_4$ was obtained by dissolving 1.39 g $FeSO_4$ in 250 cc distilled water and the second working solution of SeO_2 was obtained by dissolving 0.2774 g of SeO_2 in 250 cc distilled water. Each 20 cc of the two solutions forms the reaction mixture and this mixture was used as an electrolytic bath for all depositions. Initially, the pH value of the electrolytic bath was 2.5 ± 0.1. By adding an adjustable amount of dilute H_2SO_4 and NaOH the pH value of the electrolytic bath was adjusted to 1.5, 2.0 and 3.0 ± 0.1, respectively. If the pH value is low (i.e. below 2.0 ± 0.1), there is a rapid growth of film followed by its peeling out from the substrate. If the pH value is greater than 2.5 ± 0.1, precipitation of electrolytic bath occurs which in turn yields films with poor quality. Hence, the solution pH was fixed as 2.5 ± 0.1 in order to obtain films with better crystallinity. Electrochemical depositions were carried out using Scanning Potentiostat/Galvanostat unit (EG & G, Model 362, Princeton Applied Research, USA) employing three compartment cell consisting of ITO substrate as Working electrode, Platinum electrode as counter electrode and Saturated Calomel Electrode (SCE) as reference electrode, respectively. Before used for deposition, ITO substrates were treated for 15 min with ultrasonic waves in a bath of isopropanol and then rinsed with acetone. The SCE was kept closer to the working electrode by the use of luggin capillary arrangement. The deposition potential, bath temperature and deposition time were maintained at −450 mV versus SCE, 80 °C and 40 min, respectively. The pH value of the electrolytic bath was found to be vary in the range between 1.5 and 3.0 ± 0.1.

Electrochemical growth mechanism was analyzed using cyclic voltammetry. Cyclic voltammetric studies was carried out in a standard three compartment cell using BAS 200A electrochemical analyzer. Stylus profilometer (Mitutoyo SJ 301, Japan) was used to measure the thickness of the deposited films. An X-ray diffractometer (XPERT PRO PANalytical, Netherland) with CuK_α radiation with wavelength ($\lambda = 1.540$ Å) was used to identify the crystalline nature and phases of the deposited films. Microstructural parameters such as crystallite size, rms microstrain, dislocation density and stacking fault probability were evaluated from X-ray diffraction data using line profile analysis technique. Surface morphology and film composition were analyzed using scanning electron microscopy (JEOL JSM 840), atomic force microscopy (PSIA XE^{100}) and energy dispersive analysis by X-rays set up attached with scanning electron microscopy. Optical absorption measurements was carried out using an UV-Vis-NIR spectrophotometer (HR 2000 M/S Ocean Optics, USA) to determine the optical properties.

3. Results and Discussion

3.1. Cyclic voltammetric studies

Electrodeposition of $FeSe_2$ thin films has been carried out potentiostatically on ITO substrates from an aqueous acidic bath containing $FeSO_4$ and SeO_2. The electrochemical reactions involving in the co-deposition of Fe, Se and $FeSe_2$ are described as follows [14]

$$Fe^{2+} + 2e^- \rightarrow Fe, \quad E^0_{Fe} = -447\,mV \tag{1}$$

$$E_{Fe} = E^0_{Fe} + \left[\frac{RT}{2F}\right] \ln\left[\frac{a^{2+}_{Fe}}{a_{Fe}}\right]$$

$$SeO_2 + H_2O + 4H^+ + 4e^- \rightarrow Se + 3H_2O, \quad E^0_{Se} = 740\,mV \tag{2}$$

$$E_{Se} = E^0_{Se} + \left[\frac{RT}{4F}\right] \ln\left[\frac{a_{SeO_2}}{a_{Se}}\right] + \left[\frac{RT}{4F}\right] \ln(a_{H^+})^4$$

$$Se + 2H^+ + 2e^- \rightarrow H_2Se, \quad E^0_{Se} = -349\,mV \tag{3}$$

where E^0_{Fe} and E^0_{Se} are the standard reduction potential of Fe and Se with respect to SCE. a^{2+}_{Fe}, a_{SeO_2} are the activities of Fe and Se ions present in the electrolyte. a_{Fe}, a_{Se} are the activities of respective atoms present in the deposited films. The deposition of Fe occurs at more positive potential than their standard reduction potential by gaining free energy in compound formation. It has been reported that under potential deposition of less noble constituent here (Fe) of a compound $FeSe_2$ is brought about by the gain of free energy in the compound formation. Hence, in order to obtain co-deposition of $FeSe_2$, we have used a higher concentration of less noble constituent (here Fe) and lower concentration of noble metal (Se) in order to bring the electrode potential of two deposits closer. The mechanism of formation of $FeSe_2$ is described by the following Eq. (4):

$$Fe^{2+} + 2Se + 2e^- \rightarrow FeSe_2 \tag{4}$$

Cyclic voltammetry is a powerful analytical tool used to analyze the electrochemical reactions in an aqueous acidic bath containing $FeSO_4$, SeO_2 and the mixture of $FeSO_4$ and SeO_2 in order to find out the optimum range of potential for the preparation of Fe, Se and $FeSe_2$ thin films. Cyclic voltammetric studies have been carried out in a standard three compartment cell consists of ITO substrate as working electrode, Platinum electrode as counter electrode and SCE as reference electrode, respectively. The voltammetric curves are first scanned in the cathodic direction and the negative current density indicates cathodic current. The scan rate employed is 20 mV versus SCE. All the voltammetric curves are scanned in the potential range between −1500 and 1500 mV versus SCE. Typical cyclic voltammogram recorded for ITO glass electrode in an aqueous acidic bath containing 0.02 M $FeSO_4$ is shown in Fig. 1(a). It is observed that the cathodic current density increases gradually up to −720 mV versus SCE, there is sudden increment is observed which is indicated in Fig. 1(a). Reduction peak I observed at −900 mV versus SCE may be due to the reduction of Fe according to Eq. (1). Reduction peak II observed at −1150 mV versus SCE may be due to the reduction of the solvent. During reverse scan, an anodic peak is observed at −310 mV versus SCE which may be due to the oxidation of Fe. A hysteresis is obtained in the potential range between −700 and −1150 mV versus SCE represents that the reduction of Fe ions occurs more easily on Fe surface than that on the surface of ITO. Hence, once the substrate is covered with metal Fe the deposition of Fe occurs more easily on iron surface than that on the surface of ITO. Similar behaviour is exhibited for Fe ion on stainless steel has been reported earlier [15].

Fig. 1(b) shows the typical cyclic voltammogram recorded for ITO glass electrode in an aqueous acidic bath containing 0.01 M SeO_2. It is observed from Fig. 1(b) that a reduction wave I observed at −540 mV versus SCE may be due to the reduction of H_2SeO_3 to Se according to Eq. (2). The formation of reddish elemental selenium layer is observed on the surface of ITO at a potential −540 mV versus SCE. It is also observed that a reduction wave II observed at −980 mV versus SCE may be due to the reduction of H_2Se to Se according to Eq. (3). Similar behaviour is exhibited for metallic selenium on Ti substrate has been reported earlier [16]. Different deposition potentials such as −400 and −500 mV versus SCE have been reported earlier for Se deposition [17,18]. A slight shift in deposition potential obtained in the present work may be due to usage of different substrates and other experimental conditions such as solution pH, concentration and temperature of the electrolytic bath [1,13,16]. Cyclic voltammogram recorded for ITO glass electrode in an aqueous acidic bath containing 0.02 M $FeSO_4$ and 0.01 M SeO_2 is shown in Fig. 1(c). It is observed that a reduction wave (peak I) observed at −600 mV versus SCE may be due to cathodic reduction of H_2SeO_3 to Se according to Eq. (2). With Se being nobler, it is expected to be deposited first by the charge transfer reaction [Eq. (2)]. Reduction wave (peak II) observed at −450 mV versus SCE may be due to the formation of $FeSe_2$ films on ITO substrate according to Eq. (4). During reverse scan, an oxidation peak is observed at −360 mV versus SCE which is responsible for superimposed peaks of compound $FeSe_2$ and element Fe and hence no oxidation peak of $FeSe_2$ is found. A hysteresis is obtained in the potential range between −300 and −600 mV versus SCE thus represent the formation of

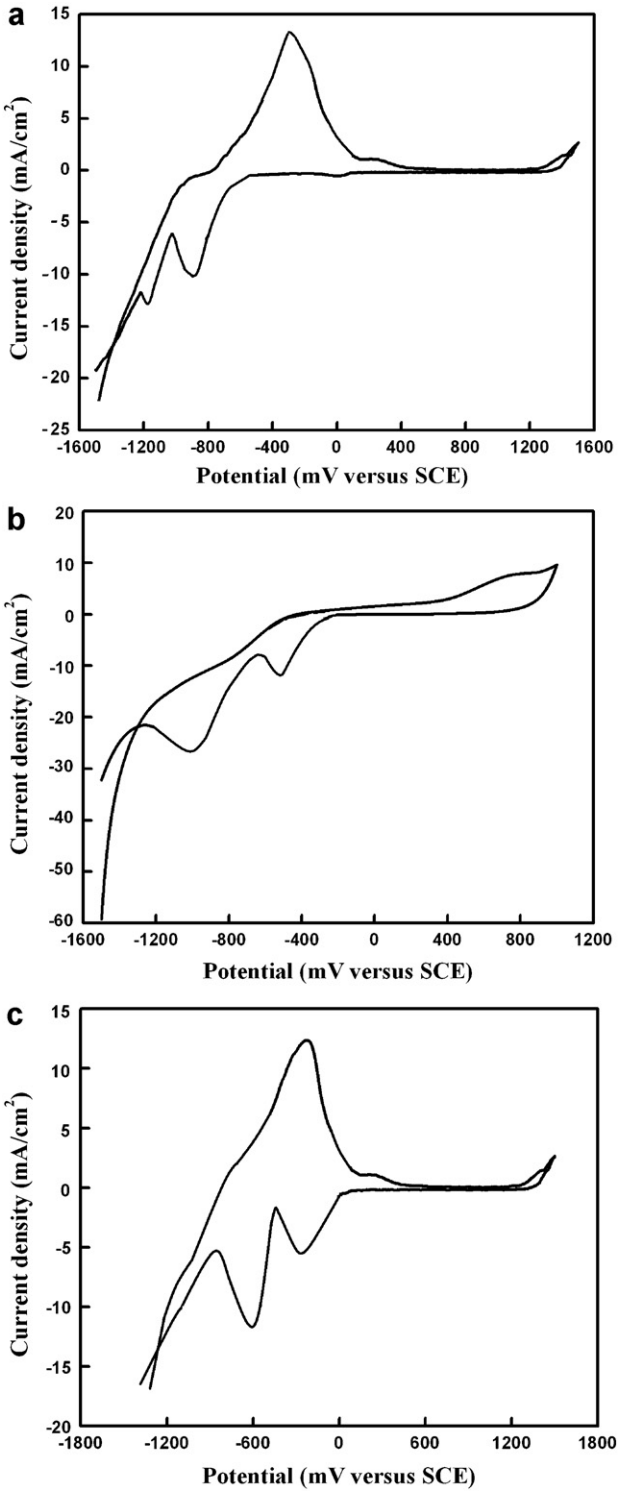

Fig. 1. (a) Cyclic voltammogram of ITO glass electrode in an aqueous electrolytic bath containing 0.02 M $FeSO_4$. (b) Cyclic voltammogram of ITO glass electrode in an aqueous electrolytic bath containing 0.01 M SeO_2. (c) Cyclic voltammogram of ITO glass electrode in an aqueous electrolytic bath containing 0.02 M $FeSO_4$ and 0.01 M SeO_2.

$FeSe_2$ occurs more easily on $FeSe_2$ surface than that on the surface of ITO. Since, the working electrode is initially covered with $FeSe_2$ instead of ITO. Results of the cyclic voltammetry shows that the potential range of −300 and −600 mV versus SCE may be used as deposition potential for the preparation of $FeSe_2$ films.

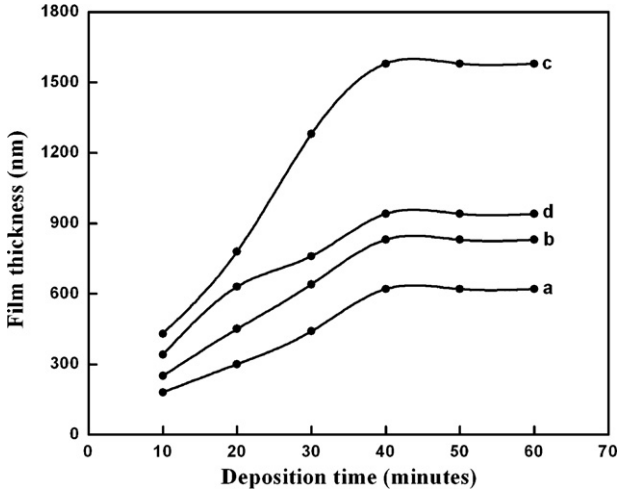

Fig. 2. (a–d) Variation of film thickness with solution pH value for $FeSe_2$ thin films prepared at various solution pH values: (a) 1.5 (b) 2.0 (c) 2.5 and (d) 3.0 ± 0.1.

3.2. Film thickness

The solution pH is one of the important key parameter which determines the film thickness, structure and composition of the deposited films. Growth of $FeSe_2$ thin films on ITO substrates has been carried out from an aqueous electrolytic bath which could be maintained at various solution pH values in the range between 1.5 and 3.0 ± 0.1. Variation of film thickness with deposition time for $FeSe_2$ thin films prepared at various solution pH values is shown in Fig. 2(a)–(d). It is observed that the film thickness increases linearly with deposition time and tend to attain its maximum value after 40 min of deposition. Further increasing the deposition time above 40 min, thickness of the deposited films remains constant up to 60 min, thereafter there is slight decrement in film thickness value is observed not shown in Fig. 2. Decrease in value of film thickness above 60 min which may be due higher rate of dissolution than the rate of deposition [19]. The pH value is maintained at 1.5 ± 0.1 the electrolytic bath has rich H^+ ion which in turn gives higher conductivity to electrolytic bath. The production of higher conductivity leads to evolution of hydrogen gas in the electrolytic bath which gives films with lower thickness value which is shown in Fig. 2(a). If the solution pH value is maintained at 3.0 ± 0.1 the formation of $Fe(OH)_2$ ion source from $FeSO_4$ and H_2O [19] leads to precipitation of electrolytic bath thus results films with lower thickness value which is shown in Fig. 2(d). The pH value is maintained at 2.5 ± 0.1 the electrolytic bath becomes transparent thus leads to the formation of film with uniform surface and well adherent to the substrates. Therefore, films with higher thickness value is obtained at a solution pH value around 2.5 ± 0.1 and at deposition time of 40 min.

3.3. Structural studies

X-ray diffraction pattern recorded for $FeSe_2$ thin films prepared on ITO substrate at various solution pH values are investigated. The solution pH is one of an important key parameter which determine the crystalline nature and stoichiometry of the deposited films. The solution pH value is less than 1.5 ± 0.1, the formation of film may be hindered due to the process of hydrogen evolution reaction, thus leads to development of poor quality films. If the solution pH value is increased above 3.0 ± 0.1, there is production of $Fe(OH)_2$ ion source thus leads to precipitation of electrolytic bath which in turn yield poor quality films. Hence, the solution pH value is fixed in the range between 1.5 and 3.0 ± 0.1 in order

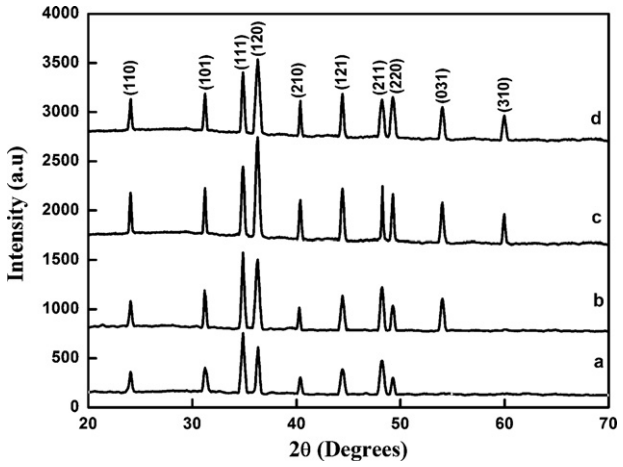

Fig. 3. (a–d) X-ray diffraction pattern of $FeSe_2$ thin films electrodeposited at various solution pH values: (a) 1.5, (b) 2.0, (c) 2.5 and (d) 3.0 ± 0.1.

to obtain films with better crystallinity. XRD pattern recorded for $FeSe_2$ thin films prepared at various solution pH values in the range between 1.5 and 3.0 ± 0.1 is shown in Fig. 3(a)–(d). XRD results represents that the deposited films are found to exhibit polycrystalline in nature with orthorhombic structure with lattice constants (a = 4.800 Å; b = 5.823 Å; c = 3.662 Å). The diffraction peaks of orthorhombic $FeSe_2$ are found at 2θ values of angles 24.06, 31.07, 34.77, 36.22, 40.20, 44.42, 48.14, 49.32, 54.09 and 59.53 corresponding to the lattice planes (1 1 0), (1 0 1), (1 1 1), (1 2 0), (2 1 0), (1 2 1), (2 1 1), (2 2 0), (0 3 1) and (3 1 0), respectively. The different peaks in the diffractogram are indexed and the corresponding values of interplanar spacing "d" are calculated and compared with standard JCPDS-ICDD file for orthorhombic $FeSe_2$ [20]. The films prepared at solution pH value around 1.5 ± 0.1 exhibit the peaks of $FeSe_2$with preferential orientation along (1 1 1) plane. If the pH value is increased there slight increment in peak height of (1 1 1) plane in addition with slight increment in peak height of (1 2 0) plane is observed which is shown in Fig. 3(b) and (c). The films prepared at solution pH value around 2.5 ± 0.1 are found to exhibit well defined crystallites with preferential orientation along (1 2 0) plane. Further increasing the solution pH value above 2.5 ± 0.1, the formation of $Fe(OH)_2$ ion from source thus leads to precipitation of electrolytic bath which in turn reduces the intensity of all the peaks as shown in Fig. 3(d). It is also observed that there is no change in crystal structure, but there is change in preferential orientation from (1 1 1) to (1 2 0) plane and increase in value of crystallinity is observed for films prepared at various solution pH values. Similar behaviour is exhibited for $CdCr_2S_4$thin films has been reported earlier [21]. The effect of deposition parameters (such as solution pH, bath temperature, deposition potential) on orientation of polycrystalline thin films are determined by evaluating the texture coefficient of the ($h\,k\,l$) plane using the following Eq. (5) [5]:

$$T_c(h\,k\,l) = \frac{I(h\,k\,l)/I_0(h\,k\,l)}{(1/N)\left[\sum_N I(h\,k\,l)/I_0(h\,k\,l)\right]} \quad (5)$$

where $T_c(h\,k\,l)$ is the texture coefficient of the ($h\,k\,l$) plane, I is the measured intensity, I_0 is the JCPDS-ICDD standard intensity and N is the number of diffraction peaks. It is observed from Eq. (5) that the value of texture coefficient approaches unity for a randomly distributed powder sample, while $T_c(h\,k\,l)$ is greater than unity when the ($h\,k\,l$) plane is preferentially oriented. Variation of texture coefficient with solution pH value for $FeSe_2$ thin films prepared at various solution pH values is shown in Fig. 4. It is observed that the value of texture coefficient is found to increase

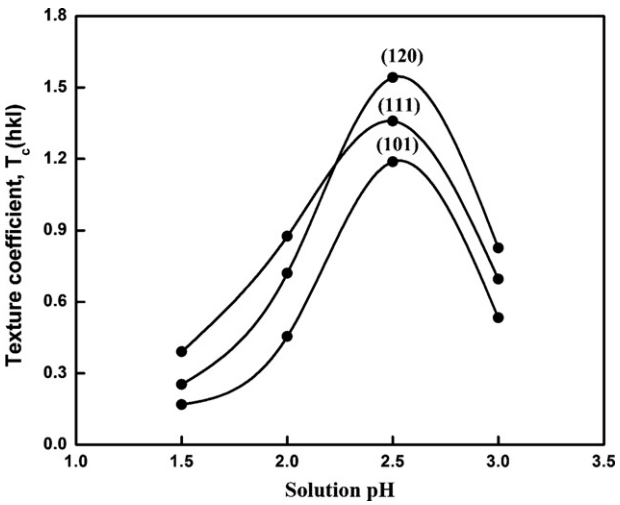

Fig. 4. Variation of texture coefficient $T_c(h\,k\,l)$ along (1 0 1), (1 1 1) and (1 2 0) planes for $FeSe_2$ thin films obtained at various solution pH values.

while increasing the solution pH value from 1.5 to 2.5 ± 0.1, thereafter its value decreases slightly which is shown in Fig. 4. The films prepared at solution pH value around 2.5 ± 0.1 has higher texture coefficient value indicates that the deposited films has higher crystallinity and well adherent to the substrates. The value of lattice constants a, b, c of orthorhombic cell is calculated using the following Eq. (6). Fig. 5 shows the variation of lattice constants with solution pH value for $FeSe_2$ thin films obtained at various solution pH values. It is observed that the lattice constant value is increased while increasing the solution pH value from 1.5 to 2.5 ± 0.1, thereafter there is slight decrement is observed which is shown in Fig. 5. Hence, the films obtained at solution pH value around 2.5 ± 0.1 have lattice constant value closer to the value given in JCPDS-ICDD file for orthorhombic $FeSe_2$ [20].

$$\frac{1}{d^2} = \left[\frac{h^2}{a^2}\right] + \left[\frac{k^2}{b^2}\right] + \left[\frac{l^2}{c^2}\right] \quad (6)$$

The average crystallite size of the deposited films are determined from FWHM data using Debye–Scherrer formula which is given in Eq. (7) [5,21]

$$P = \frac{0.9\lambda}{\beta \cos\theta_B} \quad (7)$$

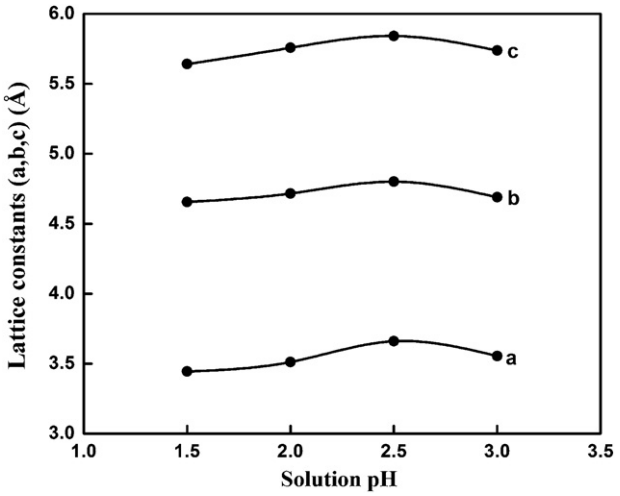

Fig. 5. Variation of lattice constants (a, b, c) with solution pH value for $FeSe_2$ thin films obtained at various solution pH values.

where α is the wavelength of CuK$_\alpha$ target used ($\lambda = 1.540$ Å), β is Full Width at Half Maximum of the peak in radian, θ_B is Bragg's diffraction angle at peak position in degrees.

The line profiles in XRD pattern are generally due to convolution of various factors like crystallite size, rms microstrain and presence of stacking faults. Line profiles in XRD pattern are used to determine the value of crystallite size, rms microstrain using X-ray line profile analysis [22]. An aggregate of distorted crystallites as a measure of crystallite size and strain could affect the variance in X-ray diffraction line profiles. Since, this method is sensitive to variation near the tails of the peaks, a careful adjustment of the background has been carried out by following the method given by Mitra and Misra [23]. For instrumental broadening the line profiles has been corrected by subtracting the variance of the corresponding profile of well-annealed $FeSe_2$ sample, because of additive effect of the variance. Assuming the broadening of the diffracted line is due to crystallite size and strain only, the variance can be written as (Eq. (8))

$$W_{2\theta} = \left[\frac{\lambda\sigma}{2\pi^2 P\cos\theta}\right] + 4\tan^2\theta\left\langle e^2\right\rangle^{1/2} \quad (8)$$

where λ is the wavelength of X-rays used, σ the angular range over which the intensity distribution is appreciable, P is the crystallite size, θ is Bragg's diffraction angle and $\langle e^2\rangle^{1/2}$ is the mean square strain. However, variance is a range sensitive parameter and consequently depends on the choice of the background level which has a marked influence on the range to be selected for integration. In fact, it is found that the diffraction lines approaches zero, rather asymptotically following an inverse square law. For such a function varying inversely as the square of the distance from the mean, the variance will be a linear function of the total range σ and can be written as $W = K\sigma + C$, where K and C are constants and are depend upon the geometrical factors and other physical conditions of the sample. Strain is defined as the restoring force acts on the surface of the film to restrict the formation of crystallites on its surface [1]. The origin of strain is related to lattice mismatch which in turn depend upon the deposition conditions (solution pH, bath temperature and deposition potential) [19]. Dislocation density is defined as the length of dislocation lines per unit volume of the crystal. Dislocation density is calculated using the following Eq. (9) [5,8,24]:

$$\rho = \frac{(3nK/F)^{1/2}\left\langle e^2\right\rangle^{1/2}}{bP} \quad (9)$$

where n be the number of dislocations on each face of the particle, K the constant depends on strain distribution, F is an interaction parameter, $\langle e^2\rangle^{1/2}$ is rms microstrain, B the Burgers vector and P the crystallite size. For Cauchy strain profiles the value of K is 25, whereas for Gaussian strain profiles, its value is 4. In the absence of extensive polygonization, dislocation density is calculated by assuming $n \approx F$, $b = d$ the interplanar spacing and $K = 4$, Now the above Eq. (9) reduces to

$$\rho = \frac{\sqrt{12}\left\langle e^2\right\rangle^{1/2}}{dP} \quad (10)$$

Stacking fault probability (α) is the fraction of layers undergoing stacking sequence faults in a given crystal and hence one fault is expected to be found in $1/\alpha$ layers [5,8]. The presence of stacking faults gives rise to a shift in peak position of different reflections with respect to ideal position of a fault-free well-annealed $FeSe_2$ sample, because of the additive effect of variance. Typical experimental profile with peak shift for most prominent reflection of $FeSe_2$ thin films prepared at different solution pH values with respect to well-annealed sample is used to evaluate the value of stacking fault probability of the deposited films. The relation

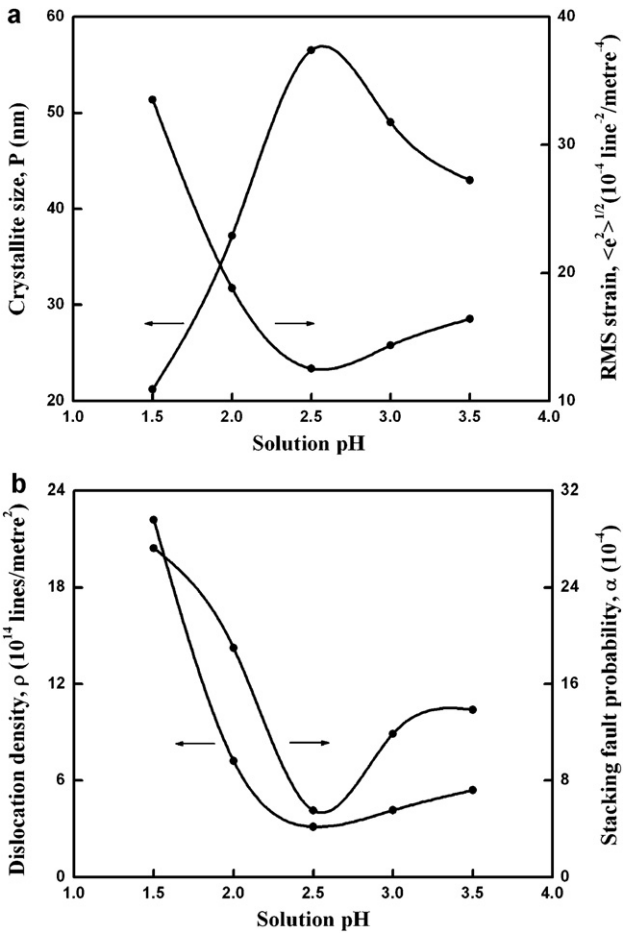

Fig. 6. (a) Variation of crystallite size and rms microstrain with solution pH value for $FeSe_2$ thin films obtained at various solution pH values. (b) Variation of dislocation density and stacking fault probability with solution pH value for $FeSe_2$ thin films obtained at various solution pH values.

connecting stacking fault probability α with peak shift $\Delta(2\theta)$ is given by Eq. (11).

$$\alpha = \left[\frac{2\pi^2}{45\sqrt{3}}\right]\left[\frac{\Delta(2\theta)}{\tan\theta_{hkl}}\right] \quad (11)$$

Using the above Eq. (11) stacking fault probability is calculated by measuring the peak shift with the well-annealed sample. X-ray diffraction pattern of $FeSe_2$ thin films electrodeposited at various solution pH values in the range between 1.5 and 3.0 ± 0.1 are recorded. Crystallite size of the deposited films are calculated using FWHM data and Debye–Scherrer formula. The rms microstrain $\langle e^2\rangle^{1/2}$ is calculated using Eq. (8). Variation of crystallite size and rms microstrain with solution pH value for $FeSe_2$ thin films obtained at various solution pH values is shown in Fig. 6(a). It is observed that the value of crystallite size is found to increase and the value of rms microstrain is found to decrease while increasing the solution pH value from 1.5 to 2.5 ± 0.1, thereafter both of them changes vice versa. X-ray line profile analysis revealed that the crystallite size increases with solution pH value and the films prepared at solution pH value around 2.5 ± 0.1 has maximum crystallite size value which is shown in Fig. 6(a). Due to the removal of defects in the lattice strain in the film gets released and tend to attain its minimum value at solution pH value 2.5 ± 0.1. A sharp increase in crystallite size and decrease in rms microstrain with solution pH value is observed which is shown in Fig. 6(a). Such a release in rms microstrain reduced the variation of interplanar spacing thus leads to decrease in value of dislocation density and

stacking fault probability of the film and minimum values are obtained at solution pH value 2.5 ± 0.1 [Fig. 6(b)]. $FeSe_2$ films with lower rms microstrain, dislocation density and stacking fault probability improves the stoichiometry of the films which is turn causes volumetric expansion of thin films. The presence of Fe ion vacancies within the lattice causes p-type conductivity to the deposited films. Crystallinity improvement with solution pH value enhances the concentration and mobility of Fe ion vacancies within the lattice and hence reduces the resistivity of the deposited films. Studies on functional dependency of microstructural parameters on solution pH value shows that the rms microstrain, dislocation density, stacking fault probability decreases, whereas the crystallite size increases. Similar functional dependency of microstructural parameters with solution pH value for CdSe thin films has been reported earlier [1].

3.4. Surface morphology and film composition

Surface morphology of $FeSe_2$ thin films is analyzed using scanning electron microscopy and atomic force microscopy. SEM picture of $FeSe_2$ thin films prepared at different solution pH values is shown in Fig. 7(a) and (b). It is observed from Fig. 7(a) that the films prepared at solution pH value around 2.0 ± 0.1 is found to be less uniform and contain less number of grains than those films obtained at solution pH value 2.5 ± 0.1. Films obtained at solution pH value 2.5 ± 0.1 have smooth spherically shaped grains which can be distributed uniformly throughout the whole surface of the films (Fig. 7(b)). If the solution pH value is increased to 3.0 ± 0.1, the sizes of the grains are decreased uniformly not shown in figure. The sizes of the grains for films obtained at solution pH value around 2.5 ± 0.1 are found to be in the range between 0.30 and 1.15 μm.

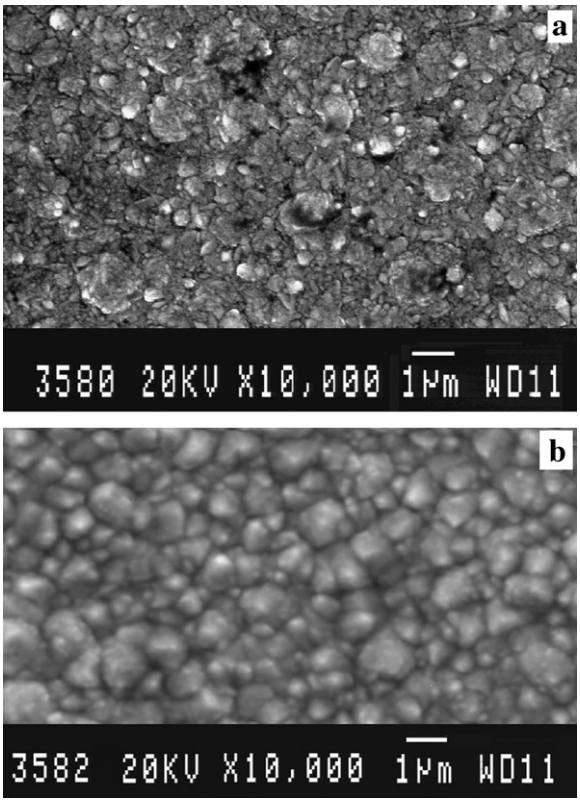

Fig. 7. SEM image of $FeSe_2$ thin films obtained at different pH solution values: (a) 2.0 and (b) 2.5 ± 0.1.

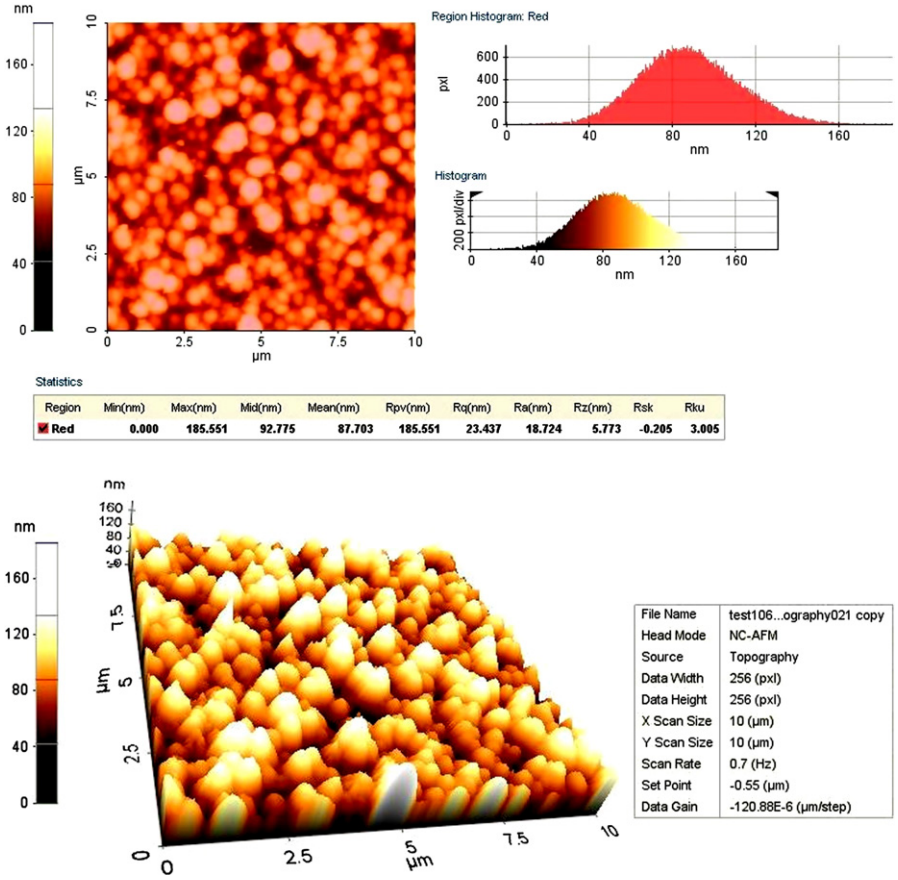

Fig. 8. AFM image of $FeSe_2$ thin films obtained at solution pH value 2.5 ± 0.1.

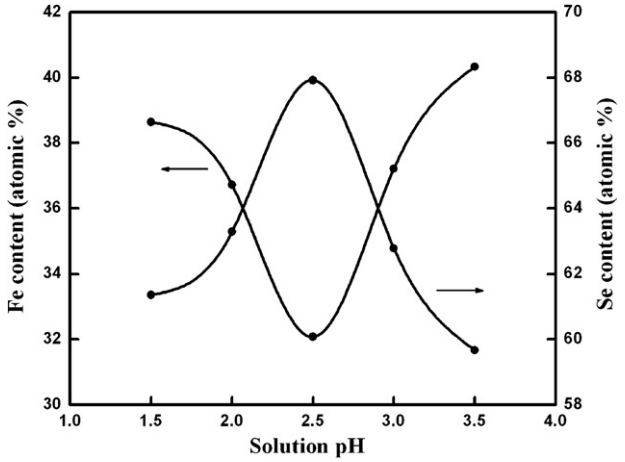

Fig. 9. Variation of Fe and Se content with solution pH value for $FeSe_2$ thin films obtained at various solution pH values.

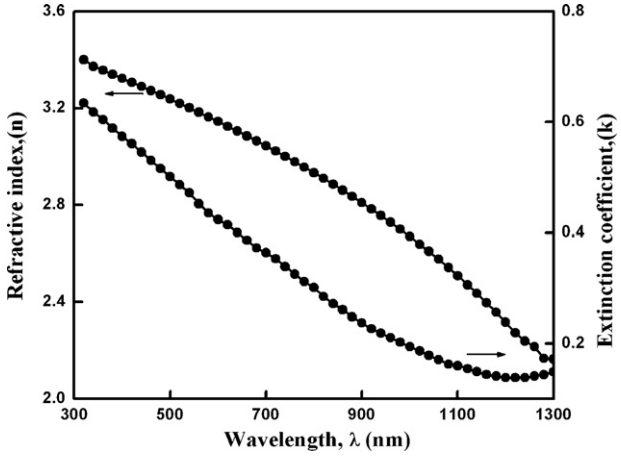

Fig. 11. Variation of refractive index (n) and extinction coefficient (k) with wavelength (λ) for $FeSe_2$ thin films.

The average size of the grains is found to be 0.69 μm. Atomic force microscope (2D and 3D) image of $FeSe_2$ thin films prepared at solution pH value 2.5 ± 0.1 is shown in Fig. 8. It is observed that the film surface has uniformly distributed hemispherical shaped grains with surface roughness (R_a) value 18.72 nm. The films prepared at solution pH value 2.5 ± 0.1 has R_a value 25.18 nm. Hence, films with lower surface roughness has been obtained at solution pH value around 2.5 ± 0.1.

The film composition is analyzed using an energy dispersive analysis by X-rays setup attached with scanning electron microscope. Variation of Fe and Se content with solution pH value for films obtained at various solution pH values is shown in Fig. 9. It is observed that the content of Fe decreased and the content of Se increased while increasing the solution pH value from 1.5 to 2.5 ± 0.1, thereafter the content of Fe increased and the content of Se decreased which is shown in Fig. 9. The atomic molar ratio (Fe:Se) of $FeSe_2$ thin film obtained at solution pH value 2.5 ± 0.1 is found to be 32.08:67.92 and is nearly (0.96) 1: 2 (2.03). This result is consistent with X-ray diffraction analysis of the sample with phase corresponds to $FeSe_2$. The atomic molar ratio of films obtained at solution pH value around 2.5 ± 0.1 which is in close agreement with the value reported earlier for $FeSe_2$ thin films [11].

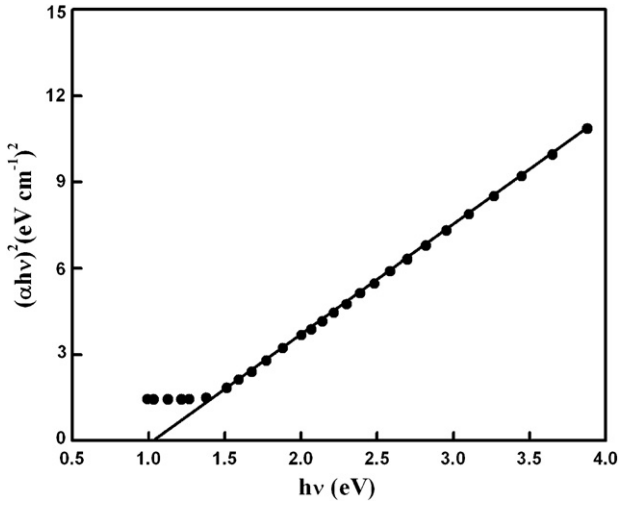

Fig. 10. Plot of $h\nu$ versus $(\alpha h\nu)^2$ for $FeSe_2$ thin films.

3.5. Optical absorption analysis

Optical transmission and absorption measurements of the deposited films are carried out in the wavelength between 300 and 1300 nm. The parameters such as absorption coefficient and band gap are determined from optical absorption and transmission measurements. The value of absorption coefficient for strong absorption region of film is calculated using the following Eq. (12) [3]:

$$\alpha = \frac{1}{t} \ln\left(\frac{A}{T}\right) \tag{12}$$

where α is the absorption coefficient in cm^{-1}, t is the thickness of the film in nm, A is the absorbance, T is the transmittance. The band gap is determined from the absorption coefficient value using the following Eq. (13) [13]:

$$\alpha h\nu = K(h\nu - E_g)^n \tag{13}$$

where α is the absorption coefficient in cm^{-1}, $h\nu$ is the photon energy in eV, E_g is an energy gap in eV and K is a constant which is related to effective masses associated with the valence and conduction band. The value of 'n' determines the type of transition present in the material. In this case $n = 1/2$ indicate that the transition involved in the material is direct allowed. A plot of $h\nu$ versus $(\alpha h\nu)^2$ for $FeSe_2$ thin films obtained at solution pH value 2.5 ± 0.1 is shown in Fig. 10. Extrapolation of linear portion of the graph to X-axis [energy ($h\nu$) axis] gives the band gap value of the material. The band gap value of the material obtained in the present work is found to be 1.03 eV which is in close agreement with the value reported earlier for $FeSe_2$ [8,9]. The value of refractive index (n) and extinction coefficient (k) are determined using the following Eqs. (14) and (15) [3]. The value of real and imaginary dielectric constants (ε_1 and ε_2) are evaluated using the following Eqs. (17) and (18):

$$n = \left(\frac{1+R}{1-R}\right) + \sqrt{\frac{4R}{(1-R)^2} - k^2} \tag{14}$$

$$k = \frac{\alpha\lambda}{4\pi} \tag{15}$$

$$\varepsilon = \varepsilon_1 + i\varepsilon_2 \tag{16}$$

$$\varepsilon_1 = n^2 - k^2 \tag{17}$$

$$\varepsilon_2 = 2nk \tag{18}$$

where n is the refractive index of the material, k is the extinction coefficient, ε_1 and ε_2 are real and imaginary dielectric constants, R is reflectance (%) and λ is the wavelength in nm.

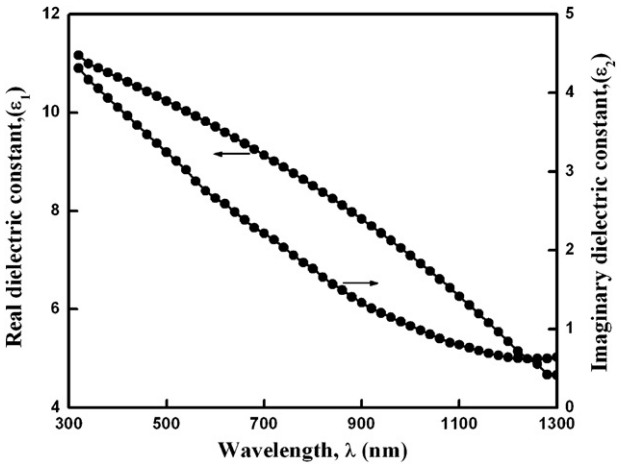

Fig. 12. Variation of real and imaginary dielectric constants (ε_1 and ε_2) with wavelength (λ) for $FeSe_2$ thin films.

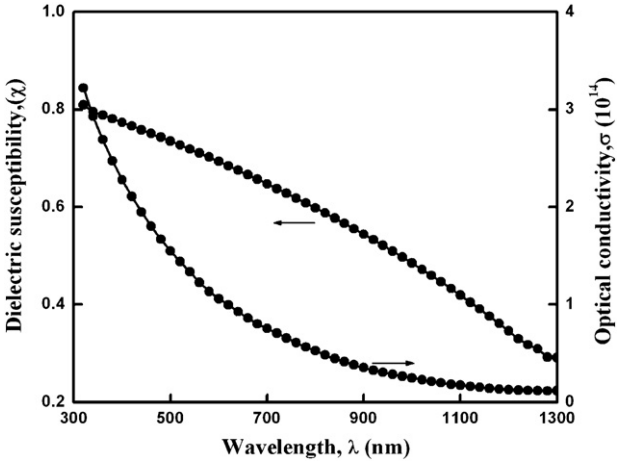

Fig. 13. Variation of dielectric susceptibility (χ) and optical conductivity (σ) with wavelength (λ) for $FeSe_2$ thin films.

Variation of refractive index (n) and extinction coefficient (k) with wavelength (λ) for typical $FeSe_2$ thin film is shown in Fig. 11. It is observed that both 'n' and 'k' are found to decrease with λ and reaches its minimum value at 1199 nm. Fig. 12 shows the variation of real and imaginary dielectric constants (ε_1 and ε_2) with wavelength (λ) for $FeSe_2$ thin film. The variation of dielectric susceptibility (χ) and optical conductivity (σ) with wavelength (λ) is shown in Fig. 13. It is noted that real, imaginary dielectric constants, dielectric susceptibility and optical conductivity are found to decrease with wavelength and reaches its minimum value at 1199 nm. The value of n, k, ε_1, ε_2, χ, σ are found to be 2.3, 0.13, 5.3, 0.61,0.34 and 0.21 corresponds to band gap value (1.03 eV) of the material. Decreasing dependence with wavelength for n, k, ε_1,ε_2, χ, σ are associated with an interband transition for photon energies smaller than the smallest band gap [25].

4. Conclusions

Thin films of $FeSe_2$ have been deposited successfully on ITO substrates using potentiostatic electrodeposition technique. The deposition potential is fixed in the range between −300 and −600 mV versus SCE using cyclic voltammetry. X-ray diffraction analysis revealed that the prepared films possess polycrystalline in nature with orthorhombic structure with preferential orientation along (1 2 0) plane. There is change in preferential orientation of the plane from (1 1 1) to (1 2 0) is observed if the solution pH value is found to vary in the range between 1.5 and 3.0 ± 0.1. The higher value of texture coefficient at solution pH value around 2.5 ± 0.1 represents that the deposited films have higher crystallinity when compared to films obtained at lower pH values. Microstructural parameters exhibit monotonic variation with solution pH value. Surface morphology shows that films with spherical and hemispherical shaped grains are obtained at solution pH value 2.5 ± 0.1. EDX analysis revealed that films with better stoichiometry is obtained at solution pH value around 2.5 ± 0.1. Optical absorption measurements indicate that the deposited film has a direct band gap value of 1.03 eV. The dispersion of n and k with frequency is similar to the behaviour reported for semiconducting chalcogenides.

Acknowledgement

One of the authors (S. Thanikaikarasan) gratefully acknowledge the Council of Scientific and Industrial Research (CSIR), New Delhi, India, for the award of Senior Research Fellowship (SRF) with File No.: 9/688 (0010) 2008 to carry out this work.

References

[1] S. Thanikaikarasan, X. Sahaya Shajan, V. Dhanasekaran, T. Mahalingam, J. Mater. Sci 46 (2011) 4034–4045.
[2] R.K. Pandey, S.N. Sahu, S. Chandra, Handbook of Semiconductor Electrodeposition, Marcel Dekker Inc, New York, 1996.
[3] S. Thanikaikarasan, T. Mahalingam, S. Lee, H. Lim, S. Velumani, J.-K. Rhee, Mater. Sci. Eng. B 174 (2010) 231–235.
[4] Kirk-Othemer, Encyclopaedia of Chemical Technology, vol. 20, New York, Wiley, 1992.
[5] S. Thanikaikarasan, T. Mahalingam, M. Raja, T. Kim, Y.D. Kim, J. Mater. Sci. Mater. Electron. 20 (2009) 727–734.
[6] G.A. Prinz, Science 282 (1998) 1660–1663.
[7] H.J. Kwon, S. Thanikaikarasan, T. Mahalingam, K.H. Park, C. Sanjeeviraja, Y.D. Kim, J. Mater. Sci. Mater. Electron. 19 (2008) 1086–1091.
[8] T. Mahalingam, S. Thanikaikarasan, R. Chandramohan, M. Raja, C. Sanjeeviraja, J.-H. Kim, Y.D. Kim, Mater. Chem. Phys. 106 (2007) 369–374.
[9] T. Harada, J. Phys. Soc. Jpn. 67 (1998) 1352–1358.
[10] B. Ouertani, J. Ouerfelli, M. Saadoun, M. Zribi, M. Ben Rabha, B. Bessais, H. Ezzaouia, Thin Solid Films 511–512 (2006) 457–462.
[11] B. Ouertani, J. Ouerfelli, M. Saadoun, B. Bessais, H. Ezzaouia, J.C. Bernede, Sol. Energy Mater. Sol. Cells 87 (2005) 501–511.
[12] N. Hamdadou, A. Khelil, M. Morsli, J.C. Bernede, Vacuum 77 (2005) 151–156.
[13] S. Thanikaikarasan, K. Sundaram, T. Mahalingam, S. Velumani, J.-K. Rhee, Mater. Sci. Eng. B 174 (2010) 242–248.
[14] M. Pourbaix, Atlas d'Equillibres Electrochimiques, Gauthier–Villar, Paris, 1963.
[15] S.M. Pawar, A.V. Moholkar, U.B. Suryavanshi, K.Y. Rajpure, C.H. Bhosale, Sol. Energy Mater. Sol. Cells 91 (2007) 560–565.
[16] C.M. Shen, X.G. Zhang, H.L. Li, Mater. Sci. Eng. B 84 (2001) 265–270.
[17] R.S. Patil, Thin Solid Films 340 (1999) 11–12.
[18] H. Saloniemi, T. Kanniainen, M. Ritala, M. Leskelä, R. Lappalainen, J. Mater. Chem. 8 (1998) 651–654.
[19] Y.G. Gudage, N.G. Deshpande, R. Sharma, J. Phys. Chem. Solids 70 (2007) 907–915.
[20] Joined Council for Powder Diffracted System – International Centre for Diffraction Data, File No.: 21-0432, USA, 2003.
[21] T. Mahalingam, S. Thanikaikarasan, V. Dhanasekaran, R. Mariappan, P. Jayamurugan, S. Velumani, J.-K. Rhee, Mater. Sci. Eng. B 174 (2010) 249–252.
[22] G.B. Mitra, Acta Crystallogr. 17 (1964) 765–766.
[23] G.B. Mitra, N.K. Misra, Br. J. Appl. Phys. 17 (1965) 1319–1328.
[24] G.K. Williamson, R.E. Smallman, Philos. Mag. 1 (1956) 34–45.
[25] S. Aksay, B. Altiokka, Phys. Stat. Sol. (c) 4 (2007) 585–588.